UCLA
COMPUTATIONAL AND APPLIED MATHEMATICS

Two-color Fourier Analysis of Iterative Algorithms for Elliptic Problems with Red/black Ordering

C.-C. Jay Kuo
Tony F. Chan

May 1988

CAM Report 88-15

Department of Mathematics
University of California, Los Angeles
Los Angeles, CA. 90024-1555

1. Introduction.

An important task of the research on parallel computation is to seek algorithms which can be conveniently implemented on vector or parallel computers. One common approach to obtain parallel iterative algorithms for the solution of partial differential equations (PDEs) is *reordering*. By reordering, we rearrange the computational sequences to increase the percentage of computations which can be done independently [26]. A crucial issue associated with reordering is how the convergence rate of an iterative algorithm is affected by a reordering scheme.

The multicolor ordering scheme for grid points provides more parallelism than the natural rowwise or columnwise ordering scheme. It is well known that by using red and black two colors to order the grid points in a checkeredboard fashion for the 5-point Laplacian, we are able to separate the coupling between any two red (or black) points so that the values at all red (or black) points can be updated simultaneously. Similarly, four colors are needed to separate the coupling between grid points of the same color for the 9-point Laplacian [1][2][3][4][19][20][21]. On either vector or parallel computers, an algorithm with the multicolor ordering is always easier to vectorize or parallelize than its naturally ordered counterpart so that such a reordering is attractive for parallel implementation. There are numerous discussions on the implementation of iterative algorithms with the red/black ordering on vector and parallel computers in the literature, for example, [2][5][8][11][19][26][27][32].

In this paper, we examine how the convergence rate of an iterative algorithm is affected by the red/black ordering. Our study includes the successive over-relaxation (SOR), symmetric successive over-relaxation (SSOR), SSOR, ILU and MILU preconditioners for preconditioned iterative methods, and multigrid (MG) methods. The convergence rates of these algorithms are analyzed by a unified approach called the *two-color Fourier analysis*. Although the two-color Fourier analysis has been used in analyzing the SOR and MG methods by the first author of this paper [19][21][22], we

believe that results for the SSOR iteration and the SSOR, ILU, MILU preconditioners are new.

Fourier or modified Fourier analysis has been used successfully to analyze numerical methods for elliptic PDE problems for years. One can conveniently study the effects of operators on Fourier modes if the numerical method of interest is applied to a simple model problem which consists of a constant-coefficient PDE on a regular domain with appropriate boundary conditions. The model problem for 2nd-order self-adjoint elliptic PDEs is the Poisson equation on a square with Dirichlet boundary conditions. For the model Poisson problem, the SOR iteration was analyzed with Fourier-like basis functions by Frankel [17] and Young [29]. Brandt used Fourier analysis to study the error smoothing property for multigrid methods [10]. Stüben and Trottenberg performed a two-grid analysis to analyze both the error smoothing and the coarse-grid correction with Fourier basis functions [28]. Fourier analysis has also been applied to the analysis of the 5-point or 9-point SOR iteration with the natural or multicolor ordering [4][19][20][21][23], preconditioners for elliptic problems with the natural ordering [13], and problems arising from the domain decomposition context [12][14].

Due to the multicolor ordering scheme, the resulting system of iteration equations is not spatially homogeneous but is *periodic* with respect to grid points. Consequently, the Fourier modes are not eigenfunctions for the multicolor system, and therefore a straightforward Fourier analysis does not apply. When these Fourier modes are operated by periodic operators, there exists a coupling between high and low frequency components. By exploiting the periodic property, we reformulate the conventional Fourier analysis as a two-color Fourier analysis. From this new viewpoint, components in the high frequency region are folded into the low frequency region so that there exist two, i.e. red and black, computational waves in the low frequency region. The coupling between the low and high conventional Fourier components is therefore

transformed into a coupling between the red and black computational waves with the same frequency in the low frequency region. With this new Fourier tool, the spectral representation of operators with the red/black ordering can be easily derived and interpreted. For the model Poisson problem, the two-color Fourier analysis is exact for Dirichlet boundary conditions and, with some modifications, is also applicable to periodic boundary conditions. The two-color Fourier analysis can be generalized to the *multicolor* Fourier analysis which applies to ordering schemes with more than two colors [20].

The determination of the optimal relaxation parameters of the SOR method with the multicolor ordering and their corresponding convergence rates for both 5-point and 9-point Laplacian operators have been intensively investigated [4][19][20][23]. It is found that if the relaxation parameters are appropriately selected, the numbers of iterations required for the red/black and natural orderings should be of the same order. In the context of MG methods, the red/black Gauss-Seidel smoother provides a better smoothing rate than the lexicographical Gauss-Seidel smoother [28]. Hence, the red/black reordering does not deteriorate the performance for these two types of algorithms.

However, the same conclusion does not apply to the SSOR iteration and preconditioned iterative methods. The optimal relaxation parameter and its corresponding convergence rate of the SSOR iteration highly depends on the ordering [7][18][31]. The naturally ordered SSOR method has the same order of convergence rate as the SOR method and can be accelerated to give a even faster convergence rate by the Chebyshev semi-iterative or conjugate gradient procedure [9][18][31]. In contrast, for the red/black ordering, it has been observed that the optimal relaxation parameter for the SSOR method is 1 so that the resulting scheme reduces to a forward and backward Gauss-Seidel relaxation which converges much slower [18]. Here, we use the two-color Fourier analysis to analyze the red/black SSOR method and determine its optimal

relaxation parameter 1 analytically. We also perform a quantitative study of the eigenstructure of the preconditioned Laplacian operator with the SSOR, ILU and MILU preconditioners. The results indicate that the condition number of the preconditioned operator with the red/black ordering is in general one order higher than that of its naturally ordered counterpart. Hence, for SSOR and preconditioned iterative methods, the convergence rate is greatly sacrificed in order to obtain more parallelism.

This paper is organized as follows. The two-color Fourier analytical approach is described and the model problem is formulated accordingly in Section 2. Section 3 analyzes the convergence rates of the SOR and SSOR iterations. Section 4 studies the eigenstructure of the preconditioned Laplacian operator with the SSOR, ILU and MILU preconditioners. Then, we perform a two-grid analysis to understand the convergence behavior of the multigrid method in Section 5. Section 6 compares the convergence rates of iterative algorithms with natural and red/black orderings. Related research work and extensions are given in Sections 7 and 8.

2. Preliminaries

2.1 Two-color Fourier analysis

Consider a 2D sequence $u_{j,k}$ defined on a grid

$$\Omega_h = \{ (jh,kh) : 0 \le j , k \le M , \quad M = \frac{1}{h} \text{ even } \} \tag{2.1}$$

with zero boundary values, i.e. $u_{j,k} = 0$ if $j,k = 0$ or M. We can expand it with Fourier series as

$$u_{j,k} = \sum_{\xi=1}^{M-1} \sum_{\eta=1}^{M-1} \hat{u}_{\xi,\eta} \sin(\xi\pi jh)\sin(\eta\pi kh) . \tag{2.2}$$

As usual we call grid point with index (j,k) the *red* or *black* point depending on whether $j+k$ is even or odd. The function $u_{j,k}$ at the red and black points defines two sequences: the red sequence $u_{r\,j,k}$ and the black sequence $u_{b\,j,k}$. They can be expanded in Fourier series respectively as

$$u_{r\,j,k} = \sum_{(\xi,\eta)\in K_r} \hat{u}_{r,\xi,\eta} \sin(\xi\pi jh)\sin(\eta\pi kh) , \qquad j+k \quad \text{even} , \tag{2.3a}$$

$$u_{b\,j,k} = \sum_{(\xi,\eta)\in K_b} \hat{u}_{b,\xi,\eta} \sin(\xi\pi jh)\sin(\eta\pi kh) , \qquad j+k \quad \text{odd} , \tag{2.3b}$$

where

$$K_b = K = \{ (\xi,\eta) \in I^2 : \ \xi+\eta \le M-1 , \ \xi , \eta \ge 1 \quad \text{or} \quad \eta = M - \xi , \ 1 \le \xi \le \frac{M}{2}-1 \} ,$$

and

$$K_r = K \cup \{ (\frac{M}{2} , \frac{M}{2}) \} .$$

It is straightforward to check that the Fourier coefficients $\hat{u}_{\xi,\eta}$, $\hat{u}_{M-\xi,M-\eta}$ in (2.2) and $\hat{u}_{r,\xi,\eta}$, $\hat{u}_{b,\xi,\eta}$ in (2.3) are related via

$$\begin{bmatrix} \hat{u}_{r,\xi,\eta} \\ \hat{u}_{b,\xi,\eta} \end{bmatrix} = \begin{bmatrix} 1 & 1 \\ 1 & -1 \end{bmatrix} \begin{bmatrix} \hat{u}_{\xi,\eta} \\ \hat{u}_{M-\xi,M-\eta} \end{bmatrix} , \quad (\xi,\eta) \in K , \tag{2.4a}$$

$$\hat{u}_{r,\xi,\eta} = \hat{u}_{\xi,\eta} , \qquad (\xi,\eta) = (\frac{M}{2},\frac{M}{2}) . \tag{2.4b}$$

We can interpret (2.4) as follows. Through the red/black decomposition (2.3), the component $(M-\xi,M-\eta)$ in the high frequency region is folded into the component (ξ,η)

in the low frequency region so that there exist two computational waves in the low frequency region. The original and the folded two-color Fourier domains are depicted in Figure 1. Note also that K_r and K_b differs only by a single element $(\frac{M}{2},\frac{M}{2})$ and, therefore, at the frequency $(\frac{M}{2},\frac{M}{2})$ we have only a scalar $\hat{u}_{r,\frac{M}{2},\frac{M}{2}}$, which is considered as the degenerate case.

2.2 Model problem: a two-wave formulation

Consider the discretized 2D Poisson equation on the square $[0,1]^2$ with grid spacing h,

$$\frac{1}{h^2}(u_{j-1,k} + u_{j+1,k} + u_{j,k-1} + u_{j,k+1} - 4u_{j,k}) = f_{j,k} , \quad 1 \le j,k \le M-1 , \qquad (2.5)$$

where $M = \frac{1}{h}$ is even and $u_{j,k}$ is given for $j,k = 0$ or M. Without loss of generality, we only consider the case where $u_{j,k}$ is zero on boundaries, since a nonzero $u_{j,k}$ on the boundary can always be moved to the right-hand side and treated as part of the driving function. In addition, since the driving term $f_{j,k}$ with $j,k = 0$ or M does not appear in (2.5), it can be viewed as zero. Consequently, the red/black Fourier series expansion (2.3) for both $u_{j,k}$ and $f_{j,k}$ are well defined. It is convenient to rewrite the equation (2.5) in terms of shift operators

$$A_{j,k}\, u_{j,k} = -\frac{h^2}{4} f_{j,k} , \qquad A_{j,k} = 1 - \frac{E_x + E_x^{-1} + E_y + E_y^{-1}}{4} , \qquad (2.6)$$

where E_x and E_y are shift operators along the x- and y- directions and $A_{j,k}$ is the local operator for the the grid point (jh,kh). We use A to denote the global operator which consists of local operators $A_{j,k}$ for grid points (jh,kh), $1 \le j,k \le M-1$.

By substituting (2.3) into (2.5) and relating the Fourier coefficients of red and black waves, we can transform (2.5) from the space domain into the red/black Fourier domain. It is a block diagonal matrix equation, in which the equation for a nondegenerate frequency (ξ,η) can be written as

$$\hat{A}(\xi,\eta)\begin{bmatrix}\hat{u}_{r,\xi,\eta}\\ \hat{u}_{b,\xi,\eta}\end{bmatrix} = -\frac{h^2}{4}\begin{bmatrix}\hat{f}_{r,\xi,\eta}\\ \hat{f}_{b,\xi,\eta}\end{bmatrix}, \quad \hat{A}(\xi,\eta) = \begin{bmatrix}1 & -\alpha_{\xi,\eta}\\ -\alpha_{\xi,\eta} & 1\end{bmatrix}, \tag{2.7a}$$

where

$$\alpha_{\xi,\eta} = \frac{\cos(\xi\pi h)+\cos(\eta\pi h)}{2}, \tag{2.7b}$$

is the Fourier transform of the space domain operator

$$\frac{E_x + E_x^{-1} + E_y + E_y^{-1}}{4}.$$

Since $(\xi,\eta) \in K$, $0 \le \alpha_{\xi,\eta} < 1$.

We will use the two-color Fourier analysis to study the convergence properties of different numerical algorithms for the model problem (2.5) with the red/black ordering. Only the nondegenerate case is considered, since the degenerate case can be analyzed similarly and it in general does not change the conclusion for each case.

3. Analysis of SOR and SSOR methods

3.1 SOR iteration

For the model problem (2.5), the red/black SOR iteration can be written as

$$\begin{aligned} u_{j,k}^{n+1/2} &= S_{r\,j,k}(\omega)u_{j,k}^{n} - P_{r\,j,k}(\omega)\frac{h^2}{4}f_{j,k} \\ u_{j,k}^{n+1} &= S_{b\,j,k}(\omega)u_{j,k}^{n+1/2} - P_{b\,j,k}(\omega)\frac{h^2}{4}f_{j,k} \end{aligned} , \tag{3.1}$$

where

$$S_{r\,j,k}(\omega) = \begin{cases} 1-\omega+\dfrac{\omega}{4}(E_x+E_x^{-1}+E_y+E_y^{-1}), & (j,k)\ \text{red} \\ 1, & (j,k)\ \text{black} \end{cases},$$

$$S_{b\,j,k}(\omega) = \begin{cases} 1, & (j,k)\ \text{red} \\ 1-\omega+\dfrac{\omega}{4}(E_x+E_x^{-1}+E_y+E_y^{-1}), & (j,k)\ \text{black} \end{cases},$$

are the local SOR iteration operators at red and black points, and

$$P_{r\,j,k}(\omega) = \begin{cases} \omega & (j,k)\ \text{red} \\ 0, & (j,k)\ \text{black} \end{cases}, \quad P_{b\,j,k}(\omega) = \begin{cases} 0, & (j,k)\ \text{red} \\ \omega & (j,k)\ \text{black} \end{cases},$$

can be viewed as the local injection operators at red and black points scaled by the parameter ω. As before, we denote their corresponding global operators by S_r, S_b, P_r and P_b respectively.

By using the red/black Fourier series expansion (2.3), we can transform (3.1) from the space domain to the frequency domain and obtain a block diagonal matrix equation. For each nondegenerate frequency (ξ,η), the iteration equation can be written as

$$\begin{aligned} \begin{bmatrix} \hat{u}_{r,\xi,\eta}^{n+1} \\ \hat{u}_{b,\xi,\eta}^{n+1} \end{bmatrix} &= \hat{S}_b(\xi,\eta,\omega)\,\hat{S}_r(\xi,\eta,\omega)\begin{bmatrix} \hat{u}_{r,\xi,\eta}^{n} \\ \hat{u}_{b,\xi,\eta}^{n} \end{bmatrix} - \frac{h^2}{4}\left[\,\hat{S}_b(\xi,\eta,\omega)\hat{P}_r(\xi,\eta,\omega)+\hat{P}_b(\xi,\eta,\omega)\,\right]\begin{bmatrix} \hat{f}_{r,\xi,\eta} \\ \hat{f}_{b,\xi,\eta} \end{bmatrix}, \\ &= \begin{bmatrix} 1 & 0 \\ \omega\alpha_{\xi,\eta} & 1-\omega \end{bmatrix}\begin{bmatrix} 1-\omega & \omega\alpha_{\xi,\eta} \\ 0 & 1 \end{bmatrix}\begin{bmatrix} \hat{u}_{r,\xi,\eta}^{n} \\ \hat{u}_{b,\xi,\eta}^{n} \end{bmatrix} - \frac{h^2}{4}\begin{bmatrix} \omega & 0 \\ \omega^2\alpha_{\xi,\eta} & \omega \end{bmatrix}\begin{bmatrix} \hat{f}_{r,\xi,\eta} \\ \hat{f}_{b,\xi,\eta} \end{bmatrix}, \end{aligned} \tag{3.2}$$

where $\alpha_{\xi,\eta}$ is given by (2.7b).

For the error, equation (3.2) is a homogeneous equation, and the error dynamic can be completely understood by studying the SOR iteration matrices,

$$\hat{S}_{rb}\ (\xi,\eta,\omega) = \hat{S}_b(\xi,\eta,\omega)\,\hat{S}_r(\xi,\eta,\omega) = \begin{bmatrix} 1-\omega & \omega\alpha_{\xi,\eta} \\ (1-\omega)\omega\alpha_{\xi,\eta} & 1-\omega+\omega^2\alpha_{\xi,\eta}^2 \end{bmatrix}. \tag{3.3}$$

The objective is to find the optimal relaxation parameter ω^* which minimizes the spectral radius ρ of the matrix S_{rb} with respect to all possible ξ and η and its corresponding spectral radius.

To do so, let us first consider fixed ξ and η. The spectral radius $\rho_{\xi,\eta}(\omega)$ of $\hat{S}_{rb}(\xi,\eta,\omega)$ can be found by solving the quadratic equation

$$| \lambda_{\xi,\eta}(\omega) - \hat{S}_{rb}(\xi,\eta,\omega) | = \lambda_{\xi,\eta}^2 - (2 - 2\omega + \omega^2\alpha_{\xi,\eta}^2)\lambda_{\xi,\eta} + (1-\omega)^2 = 0\ ,$$

so that

$$\rho_{\xi,\eta}(\omega) = \max | \lambda_{\xi,\eta}(\omega) | = \begin{cases} \omega - 1\ , & \omega^*_{\xi,\eta} \le \omega < 2 \\ \left[\dfrac{\omega\alpha_{\xi,\eta}+[\omega^2\alpha_{\xi,\eta}^2-4(\omega-1)]^{1/2}}{2}\right]^2, & 0 < \omega \le \omega^*_{\xi,\eta} \end{cases}, \tag{3.4}$$

where

$$\omega^*_{\xi,\eta} = \frac{2}{1 + (1-\alpha_{\xi,\eta}^2)^{1/2}}\ .$$

From (3.4), it is easy to see that when $0 < \omega_{\xi,\eta} < 2$, $\rho_{\xi,\eta} < 1$. In addition, the relaxation parameter $\omega = \omega^*_{\xi,\eta}$ minimizes $\rho_{\xi,\eta}$ which takes the value $\omega^*_{\xi,\eta} - 1$.

Next, let us vary the values of ξ and η, and determine the optimal relaxation parameter for $(\xi,\eta) \in K$. Since the procedure is standard, only the results are summarized [19][30]. The optimal relaxation parameter is

$$\omega^* = \frac{2}{1 + (1-\alpha_{\xi,\eta,\max}^2)^{1/2}}\ , \qquad \alpha_{\xi,\eta,\max} = \max_{(\xi,\eta)\in K} \alpha_{\xi,\eta} = \cos(\pi h)\ , \tag{3.5}$$

where $\alpha_{\xi,\eta,\max}$ occurs at the lowest frequency $(\xi,\eta) = (1,1)$. Its corresponding spectral radius is

$$\rho^*_{SOR}(\text{ red/black ordering ; Dirichlet b.c. }) = \omega^* - 1 \approx 1 - 2\pi h\ . \tag{3.6}$$

With this optimal relaxation parameter ω^*, the eigenvalues of S_{rb} are distributed along

a circle of radius $\omega^* - 1$ in the complex plane. The results in (3.5) and (3.6) are in fact special cases of the general SOR theory by Young [29][30].

3.2 SSOR iteration

One SSOR iteration with the red/black ordering consists of one red/black SOR iteration followed by one black/red SOR iteration. Hence, the corresponding iteration matrix can be written as

$$\hat{S}_{SSOR}\ (\xi,\eta,\omega) = \hat{S}_r(\xi,\eta,\omega)\ \hat{S}_b(\xi,\eta,\omega)\ \hat{S}_b(\xi,\eta,\omega)\ \hat{S}_r(\xi,\eta,\omega)\ , \tag{3.7}$$

where $\hat{S}_r$ and $\hat{S}_b$ are given in (3.2). Note that we can rewrite the frequency domain red/black SOR iteration matrix as

$$\hat{S}_b(\xi,\eta,\omega)\ \hat{S}_r(\xi,\eta,\omega) = I - \omega\ (\ I - \omega\hat{L}(\xi,\eta)\ )^{-1}\ \hat{A}(\xi,\eta)\ , \tag{3.8}$$

where I is the 2 by 2 identity matrix, $\hat{A}(\xi,\eta)$ is the frequency domain Laplacian defined by (2.7a), and

$$\hat{L}(\xi,\eta) = \begin{bmatrix} 0 & 0 \\ \alpha_{\xi,\eta} & 0 \end{bmatrix}.$$

Similarly, the frequency domain black/red SOR iteration matrix can be written

$$\hat{S}_r(\xi,\eta,\omega)\ \hat{S}_b(\xi,\eta,\omega) = I - \omega\ (\ I - \omega\hat{U}(\xi,\eta)\ )^{-1}\ \hat{A}(\xi,\eta)\ , \tag{3.9}$$

where $\hat{U}(\xi,\eta) = \hat{L}^T(\xi,\eta)$. Combining (3.7)-(3.9), we have

$$\hat{S}_{SSOR}\ (\xi,\eta,\omega) = I - \omega(2-\omega)\ (\ I - \omega\hat{U}(\xi,\eta)\ )^{-1}\ (\ I - \omega\hat{L}(\xi,\eta)\ )^{-1}\ \hat{A}(\xi,\eta)\ . \tag{3.10}$$

The optimal relaxation parameter is selected to minimize the spectral radius of S_{SSOR}, or equivalently, to maximize the smaller eigenvalue of the second term in the right-hand-side of (3.10). It is easy to see that $\omega(2-\omega)$ takes the maximum value when $\omega = 1$. In addition, it will be shown in Section 4.1 that $\omega = 1$ maximizes the smaller eigenvalue $\lambda_{\xi,\eta,-}$ of the matrix

$$(\ I - \omega\hat{U}(\xi,\eta)\ )^{-1}\ (\ I - \omega\hat{L}(\xi,\eta)\ )^{-1}\ \hat{A}(\xi,\eta)\ ,$$

for $(\xi,\eta) \in K$. Thus, the optimal relaxation parameter is 1, with which the spectral radius of the SSOR iteration becomes

$$\rho^*_{SSOR}(\text{ red/black ordering ; Dirichlet b.c. }) = \cos^2\pi h \approx 1 - \pi^2 h^2\ . \tag{3.11}$$

4. Analysis of preconditioners

An important class of iterative methods for solving elliptic PDEs is obtained by first preconditioning the system of equations and then solving the preconditioned system with effective iterative methods [9]. One such example is the preconditioned conjugate gradient (PCG) method. It is well known that the rate of convergence of a preconditioned iterative method system depends on the condition number as well as the distribution of the eigenvalues of the preconditioned system [7][9].

For the model Poisson problem with the natural ordering, Chan and Elman [13] used Fourier analysis with basis functions $e^{i2\pi\xi jh}e^{i2\pi\eta kh}$ to obtain all eigenvalues of the preconditioned Laplacian with the ILU, MILU, SSOR and ADDKR preconditioners. Here, we analyze the eigenstructure of the model problem (2.5) with the red/black ordering. The two-color Fourier analysis with basis functions $\sin(\xi\pi jh)\sin(\eta\pi kh)$ is used to determine all eigenvalues of the preconditioned system. Note that different basis functions are chosen for these two orderings. For the red/black ordering, since the stencils of iterative operators are symmetric, either sine or complex sinusoidal functions can be conveniently used as basis functions, and the resulting analysis is exact for Dirichlet and periodic boundary conditions respectively. For the natural ordering, since the stencils of iterative operators are usually not symmetric, only the complex sinusoidal functions can be conveniently used as basis functions. Such an analysis is exact for periodic boundary conditions but in general not exact for Dirichlet boundary conditions. However, experimental results indicate that the eigenvalue distribution of the preconditioned system is not sensitive to the change of boundary conditions [13].

Three different types of preconditioners, i.e. the SSOR, ILU and MILU preconditioners, are studied below.

4.1 SSOR preconditioner

Suppose that we define the local operators $L_{j,k}$ and $U_{j,k}$ as

$$L_{j,k} = \begin{cases} 0\,, & (j,k)\ \text{red} \\ \frac{1}{4}(\,E_x + E_x^{-1} + E_y + E_y^{-1}\,)\,, & (j,k)\ \text{black} \end{cases}, \tag{4.1a}$$

$$U_{j,k} = \begin{cases} \frac{1}{4}(\,E_x + E_x^{-1} + E_y + E_y^{-1}\,)\,, & (j,k)\ \text{red} \\ 0\,, & (j,k)\ \text{black} \end{cases}. \tag{4.1b}$$

It is easy to see that their corresponding global operators L and U are related to A by $A = I - (\,L + U\,)$. Then, the global SSOR preconditioner with the red/black ordering is in form [6]

$$Q_S = (\,I - \omega L\,)\,(\,I - \omega\, U\,)\,. \tag{4.2}$$

where ω is the relaxation parameter. By using the two-color Fourier analysis, we can transform it to the frequency domain

$$\hat{Q}_S(\xi,\eta) = \begin{bmatrix} 1 & 0 \\ -\omega\alpha_{\xi,\eta} & 1 \end{bmatrix} \begin{bmatrix} 1 & -\omega\alpha_{\xi,\eta} \\ 0 & 1 \end{bmatrix} = \begin{bmatrix} 1 & -\omega\alpha_{\xi,\eta} \\ -\omega\alpha_{\xi,\eta} & 1+\omega^2\alpha_{\xi,\eta}^2 \end{bmatrix}, \tag{4.3}$$

where $\alpha_{\xi,\eta}$ is defined in (2.7b). From (2.7) and (4.3), we find that the SSOR preconditioned operator $Q_S^{-1}A$ has the spectral representation

$$\hat{Q}_S^{-1}(\xi,\eta)\hat{A}\,(\xi,\eta) = \begin{bmatrix} 1-\omega\alpha_{\xi,\eta}^2+\omega^2\alpha_{\xi,\eta}^2 & -\alpha_{\xi,\eta}+\omega\alpha_{\xi,\eta}-\omega^2\alpha_{\xi,\eta}^3 \\ -\alpha_{\xi,\eta}+\omega\alpha_{\xi,\eta} & 1-\omega\alpha_{\xi,\eta}^2 \end{bmatrix}, \tag{4.4}$$

which has two eigenvalues

$$\lambda_{\xi,\eta,\pm} = 1 - \frac{1}{2}\alpha_{\xi,\eta}^2\omega(2-\omega) \pm \frac{1}{2}\alpha_{\xi,\eta}[\alpha_{\xi,\eta}^2\omega^2(2-\omega)^2 - 4\omega(2-\omega) + 4\,]^{1/2}\,. \tag{4.5}$$

When $0 < \omega < 2$, the eigenvalues $\lambda_{\xi,\eta}$ are not only real but also positive and, therefore, $Q_S^{-1}A$ corresponds to a symmetric positive definite (SPD) matrix suitable for the conjugate gradient method. The condition number κ of the operator $Q_S^{-1}A$ is determined by

$$\kappa(Q_S^{-1}A) = \frac{\max\limits_{\xi,\eta} |\ \lambda_{\xi,\eta,+}\ |}{\min\limits_{\xi,\eta} |\ \lambda_{\xi,\eta,-}\ |}\,,$$

which is to be minimized by choosing an appropriate relaxation parameter $0 < \omega < 2$.

To determine the condition number, it is convenient to rewrite (4.5) as

$$\lambda_{\pm}(x,y) = 1 - \frac{x^2 y}{2} \pm \frac{x}{2}\,(x^2y^2 - 4y + 4)^{1/2},$$

where $0 \le x = \alpha_{\xi,\eta} < 1$ and $0 < y = \omega(2-\omega) \le 1$. By taking the partial derivative with respect to y for $\lambda_{\pm}$, we find that λ_+ and λ_- are monotonically decreasing and increasing respectively for given x. So, $y = 1$ gives the smallest condition number and the optimal relaxation parameter is 1. The corresponding eigenvalues in (4.5) become

$$\lambda_{\xi,\eta,\pm} = 1 - \frac{1}{2}\alpha_{\xi,\eta}^2 \pm \frac{1}{2}\alpha_{\xi,\eta}^2 . \tag{4.6}$$

The maxima of $\lambda_{\xi,\eta,+}$ are 1, and the minimum of $\lambda_{\xi,\eta,-}$ is $1 - \cos^2(\pi h) \approx \pi^2 h^2$, which occurs at $(\xi,\eta) = (1,1)$. Therefore, the condition number of the SSOR preconditioned Laplacian is

$$\kappa(Q_S^{-1}A) = \frac{1}{1-\cos^2(\pi h)} \approx \frac{1}{\pi^2 h^2} = O(\frac{1}{h^2}) . \tag{4.7}$$

The distribution of the eigenvalues $\lambda_{\xi,\eta,\pm}$ given by (4.6) is plotted as function of $\alpha_{\xi,\eta}$ in Figure 2(a). The surface plot of the eigenvalue $\lambda_{\xi,\eta,-}$ as function of $(\theta,\phi) = (\xi\pi h, \eta\pi h)$ is presented in Figure 2(b). Note that the condition number of the Laplacian is $\frac{1}{1-\cos(\pi h)} = \frac{2}{\pi^2 h^2}$. Hence, for small h, the red/black SSOR preconditioner only reduces the condition number of the original matrix by a factor of 2.

4.2 ILU preconditioner

An incomplete factorization for a matrix can be determined by imposing specific sparse patterns and constraints for elements on the factorizing matrices as well as their product. Since the construction of a matrix specifies not only a system of equations but also an ordering scheme for the variables, the incomplete factorization highly depends on the ordering. In this and the following sections, we study the spectra of two well-known preconditioners, i.e. the ILU and MILU preconditioners, which are constructed based on incomplete lower/upper triangular factorization.

The ILU and MILU factorizations were originally defined in [24] and [16] respectively. We summarize their definitions as follows. It is required for both the ILU and

MILU factorizations that the factorizing lower and upper triangular matrices have the same sparse patterns as the lower and upper triangular parts of the original matrix. Besides, the off-diagonal nonzero elements of the original matrix should have the same values as the corresponding elements of the product matrix. The major difference between them is that the ILU factorization requires that the diagonal elements of the original and product matrices be also the same while the MILU factorization requires that the row sum of the product matrix differ from the row sum of the original matrix by a small quantity $\delta = ch^2$, where c is a constant independent of h.

The factorizing operators generally have different coefficients associated with different grid points due to the boundary effects. However, these coefficients usually reach their asymptotic constant values for the region sufficiently far away from boundaries. In the following analysis, we ignore the boundary effect and analyze the preconditioned system with the asymptotic preconditioners.

For the ILU factorization, consider the local operators $L_{j,k}$ and $U_{j,k}$

$$L_{j,k} = \begin{cases} 1 , & (j,k) \text{ red} \\ 1 - \frac{1}{4}(E_x + E_x^{-1} + E_y + E_y^{-1}) , & (j,k) \text{ black} \end{cases}$$

$$U_{j,k} = \begin{cases} 1 - \frac{1}{4}(E_x + E_x^{-1} + E_y + E_y^{-1}) , & Q_{M(j,k)} \text{ red} \\ \frac{3}{4} , & (j,k) \text{ black} \end{cases}$$

With the red/black ordering, the global operators L and U correspond to lower and upper triangular matrices. Since the operator $L_{j,k}$ (or $U_{j,k}$) has nonzero coefficients for the terms 1, E_x, E_x^{-1}, E_y and E_y^{-1}, the sparse pattern of L (or U) is the same as that of the original matrix A for the lower (or upper) triangular part. We define the global operator Q_I to be the product of the lower and upper global operators,

$$Q_I = L\ U\ .$$

Let $R = Q_I - A$. Then, R consists of the local operators

$$R_{j,k} = \begin{cases} 0\,, & (j,k) \text{ red} \\ \frac{1}{8}(E_x E_y + E_x^{-1}E_y + E_x E_y^{-1} + E_x E_y^{-1}) + \frac{1}{16}(E_x^2 + E_x^{-2} + E_y^2 + E_y^{-2})\,, & (j,k) \text{ black} \end{cases},$$

for points not close to the boundaries. Note that the operator $(Q_I)_{j,k}$ has the same coefficients as $A_{j,k}$ (i.e. $R_{j,k} = 0$) for terms corresponding to 1, E_x, E_x^{-1}, E_y and E_y^{-1}, which constitute the nonzero terms for the sparse matrix A. Note that the sparse patterns of L, U and Q_I described above consist with the sparsity conditions required by the ILU factorization. We conclude that Q_I is the desired ILU preconditioner for the Laplacian with the red/black ordering.

In the Fourier domain, we have

$$\hat{Q}_I(\xi,\eta) = \begin{bmatrix} 1 & 0 \\ -\alpha_{\xi,\eta} & 1 \end{bmatrix} \begin{bmatrix} 1 & -\alpha_{\xi,\eta} \\ 0 & \frac{3}{4} \end{bmatrix} = \begin{bmatrix} 1 & -\alpha_{\xi,\eta} \\ -\alpha_{\xi,\eta} & \frac{3}{4} + \alpha_{\xi,\eta}^2 \end{bmatrix}.$$

Therefore, the ILU preconditioned operator $Q_I^{-1}A$ has the spectral representation

$$\hat{Q}_I^{-1}(\xi,\eta)\hat{A}(\xi,\eta) = \begin{bmatrix} 1 & \frac{1}{3}\alpha_{\xi,\eta} - \frac{4}{3}\alpha_{\xi,\eta}^3 \\ 0 & \frac{4}{3}(1 - \alpha_{\xi,\eta}^2) \end{bmatrix},$$

which has two real and positive eigenvalues

$$\lambda_{\xi,\eta} = 1\,,\ \frac{4}{3}(1 - \alpha_{\xi,\eta}^2)\,. \tag{4.8}$$

The condition number of the ILU preconditioned Laplacian can be determined by

$$\kappa(Q_I^{-1}A) = \frac{\max\limits_{\xi,\eta} |\lambda_{\xi,\eta}|}{\min\limits_{\xi,\eta} |\lambda_{\xi,\eta}|} = \frac{\max\limits_{\xi,\eta} \frac{4}{3}(1 - \alpha_{\xi,\eta}^2)}{\min\limits_{\xi,\eta} \frac{4}{3}(1 - \alpha_{\xi,\eta}^2)} \approx \frac{1}{\pi^2 h^2} = O(\frac{1}{h^2})\,, \tag{4.9}$$

where the maximum value $\frac{4}{3}$ occurs when $\alpha_{\xi,\eta} = 0$ and the minimum value $\frac{4}{3}[1-\cos^2(\pi h)]$ occurs at $(\xi,\eta) = (1,1)$. By the ILU preconditioning, we reduce the condition number of A approximately by a factor of 2. The distribution of the two eigenvalues $\lambda_{\xi,\eta}$ (4.8) as function of $\alpha_{\xi,\eta}$ and the surface plot of the eigenvalue $\frac{4}{3}(1-\alpha_{\xi,\eta}^2)$ as function of $(\theta,\phi) = (\xi\pi h, \eta\pi h)$ are shown in Figures 3(a) and 3(b). The corresponding

plot of the natural ordering case can be found in [13], where the condition number of A is reduced approximately by a factor $2(2+\sqrt{2})$.

4.3 MILU preconditioner

For the MILU factorization, consider the local operators $L_{j,k}$ and $U_{j,k}$

$$L_{j,k} = \begin{cases} 1+\delta\,, & (j,k) \text{ red} \\ 1+\delta-\dfrac{1}{1+\delta}-\dfrac{1}{4}(E_x+E_x^{-1}+E_y+E_y^{-1})\,, & (j,k) \text{ black} \end{cases},$$

$$U_{j,k} = \begin{cases} 1-\dfrac{1}{4(1+\delta)}(E_x+E_x^{-1}+E_y+E_y^{-1})\,, & (j,k) \text{ red} \\ 1\,, & (j,k) \text{ black} \end{cases},$$

where $\delta = ch^2$. The sparse patterns of L and U given above are the same as those for the ILU factorization, but they have different weighting coefficients. The global operator Q_M is defined to be the product of the lower and upper global operators,

$$Q_M = L\ U\ .$$

Let $R = Q_M - A$. Then, R consists of the local operators

$$R_{j,k} = \begin{cases} \delta\,, & (j,k) \text{ red} \\ \delta+\dfrac{1}{1+\delta}[-\dfrac{3}{4}+\dfrac{1}{8}(E_xE_y+E_x^{-1}E_y+E_xE_y^{-1}+E_x^{-1}E_y^{-1})+\dfrac{1}{16}(E_x^2+E_x^{-2}+E_y^2+E_y^{-2})\,] & (j,k) \text{ black} \end{cases},$$

for points not close to the boundaries. Note that $(Q_M)_{j,k}$ has the same coefficients as $A_{j,k}$ $(R_{j,k}=0)$ for terms E_x, E_x^{-1}, E_y and E_y^{-1}, which are nonzero off-diagonal entries of the matrix A. However, unlike the ILU case, the matrices A and Q_M do not have the same diagonal entries. Instead, we find that the sum of coefficients of the local error operator $R_{j,k}$ equals to δ. This implies that the row sums of matrices A and Q_M differ by a quantity of δ. By definition, Q_M is the MILU preconditioner for the Laplacian with the red/black ordering.

The Fourier transform of Q_M gives

$$\hat{Q}_M(\xi,\eta) = \begin{bmatrix} 1+\delta & 0 \\ -\alpha_{\xi,\eta} & 1+\delta-\frac{1}{1+\delta} \end{bmatrix} \begin{bmatrix} 1 & -\frac{\alpha_{\xi,\eta}}{1+\delta} \\ 0 & 1 \end{bmatrix} = \begin{bmatrix} 1+\delta & -\alpha_{\xi,\eta} \\ -\alpha_{\xi,\eta} & 1+\delta+\frac{\alpha_{\xi,\eta}^2-1}{1+\delta} \end{bmatrix}.$$

Hence, the MILU preconditioned operator has the spectral representation

$$\hat{Q}_M^{-1}(\xi,\eta)\hat{A}(\xi,\eta) = \frac{1}{\delta(\delta+2)} \begin{bmatrix} \delta(1+\frac{1-\alpha_{\xi,\eta}^2}{1+\delta}) & -\alpha_{\xi,\eta}(\delta+\frac{\alpha_{\xi,\eta}^2-1}{1+\delta}) \\ -\alpha_{\xi,\eta}\delta & 1+\delta-\alpha_{\xi,\eta}^2 \end{bmatrix},$$

which has the eigenvalues

$$\lambda_{\xi,\eta,\pm} = \frac{2\delta(1+\delta)+(1-\alpha_{\xi,\eta}^2)(1+2\delta)\pm[(1-\alpha_{\xi,\eta}^2-2\delta\alpha_{\xi,\eta}^2)^2 + 4\delta^3\alpha_{\xi,\eta}^2(2+\delta)]^{1/2}}{2\delta(1+\delta)(2+\delta)}. \qquad (4.10)$$

Note that if $\delta = 0$ (i.e. $c = 0$), $\hat{Q}_M(\xi,\eta)$ is a singular matrix which cannot be used as a preconditioner. For $c > 0$, since

$$4\delta^3\alpha_{\xi,\eta}^2(2+\delta) \ll (1-\alpha_{\xi,\eta}^2-2\delta\alpha_{\xi,\eta}^2)^2, \qquad (4.11)$$

as h goes to zero, we can simplify (4.10) as

$$\lambda_{\xi,\eta,\pm} \approx \frac{2\delta(1+\delta)+(1-\alpha_{\xi,\eta}^2)(1+2\delta)\pm(1-\alpha_{\xi,\eta}^2-2\delta\alpha_{\xi,\eta}^2)}{2\delta(1+\delta)(2+\delta)}.$$

For small h and positive c, $1-\alpha_{\xi,\eta}^2-2\delta\alpha_{\xi,\eta}^2$ is positive. So, $\lambda_{\xi,\eta,+}$ and $\lambda_{\xi,\eta,-}$ are the larger and smaller eigenvalues respectively. Then, the condition number of the MILU preconditioned Laplacian is found to be

$$\kappa(Q_M^{-1}A) = \frac{\max\limits_{\xi,\eta} | \lambda_{\xi,\eta,+} |}{\min\limits_{\xi,\eta} | \lambda_{\xi,\eta,-} |} \approx \frac{\max\limits_{\xi,\eta} \delta(1-\alpha_{\xi,\eta}^2+\delta)+(1-\alpha_{\xi,\eta}^2)(1+\delta)}{\delta(2+\delta)} \approx \frac{1}{2ch^2} = O(\frac{1}{h^2}) \qquad (4.12)$$

where the maximum value $(1+\delta)^2$ occurs when $\alpha_{\xi,\eta} = 0$.

For fixed h, the optimal parameter c and the corresponding condition number $\kappa(Q_M^{-1}A)$ can be determined by solving (4.10) numerically. The condition number $\kappa(Q_M^{-1}A)$ is plotted as function of the parameter c with different h in Figure 4. For small c ($c \le 5$), the condition number behaves very close to $\frac{1}{2ch^2}$ as predicted by (4.12). For $c \gg 5$, the condition (4.11) is no more valid, and we see that $\kappa(Q_M^{-1}A)$ remains approximately the same for a wide range of c. Thus, the condition number is

not sensitive to the selection of the relaxation parameter, as long as it is in the appropriate range. For these values of h used in Figure 4, the optimal condition number is achieved when $c \approx 5$. Thus, we know from the above analysis that the condition number of the original Laplacian is improved approximately by a factor of $\frac{4c}{\pi^2} \approx 2$. This improvement is about the same as that for the red/black ordered SSOR and ILU preconditioners.

The distribution of the eigenvalues $\lambda_{\xi,\eta,\pm}$ given by (4.10) with $\delta = 5h^2$ (i.e. $c = 5$) is plotted as function of $\alpha_{\xi,\eta}$ in Figure 5(a). Note that the eigenvalue $\lambda_{\xi,\eta,-}$ is nearly a constant. The surface plot of the eigenvalue $\lambda_{\xi,\eta,+}$ as function of $(\theta,\phi) = (\xi\pi h, \eta\pi h)$ is shown in Figure 5(b).

5. Analysis of the multigrid (MG) method

Multigrid (MG) methods provide one of the most effective ways for solving elliptic PDEs. The multigrid iteration is often modeled by a $(h,2h)$ two-grid iteration process so that its mechanism can be easily understood. The efficiency of the two-grid (or multigrid) iteration is based on a simple idea - to treat error components of low and high frequencies differently. Suppose that we partition the Fourier domain into two regions of which the low frequency region contains $1 \le \xi, \eta < \frac{M}{2}$ and the high frequency region contains $\frac{M}{2} \le \xi \le M-1$ or $\frac{M}{2} \le \eta \le M-1$. The mechanism of the two-grid iteration with the damped Jacobi or the lexicographical (naturally ordered) Gauss-Seidel smoother can be easily explained. That is, the high frequency error is smoothed at the fine grid while the low frequency error is corrected at the coarse grid. Thus, the study of the error smoothing over the high frequency region provides a rough estimate of the convergence behavior of the multigrid iteration. This is known as the *smoothing rate analysis* [10].

It is known that MG with the red/black Gauss-Seidel smoother performs better than MG with the damped Jacobi or the lexicographical Gauss-Seidel smoother for the model Poisson problem [28]. However, the efficiency of the red/black Gauss-Seidel smoother cannot be appropriately explained by the smoothing rate analysis. To see this, let us examine the red/black Gauss-Seidel iteration matrix in the two-color Fourier domain,

$$\hat{S}_{RBGS}\ (\xi,\eta) = \begin{bmatrix} 0 & \alpha_{\xi,\eta} \\ 0 & \alpha^2_{\xi,\eta} \end{bmatrix},$$

which is obtained from (3.3) with $\omega = 1$. The smoothing rate μ is usually defined as

$$\mu = \max_{(\xi,\eta)\in K_{high}} \rho[\hat{S}_{RBGS}(\xi,\eta)] = \cos^2(\pi h) \approx 1 - \pi^2 h^2,$$

where

$$K_{high} = \{\ (\xi,\eta) : \xi, \eta \in I,\ \frac{M}{2} \le \xi \le M-1 \text{ or } \frac{M}{2} \le \eta \le M-1\ \},$$

and the maximum value occurs at $\xi = \eta = M-1$. This shows that the red/black Gauss-Seidel smoother has a very poor smoothing rate as compared to the natural ordering case for which the smoothing rate is $\frac{1}{2}$ [10].

Since the smoothing rate analysis does note explain how the MG method with the red/black Gauss-Seidel smoothing works, it is essential to perform a complete two-grid analysis, which includes both smoothing and coarse-grid correction. A two-grid analysis was performed by Stüben and Trottenberg by using modified Fourier analysis [28]. Here, we use the framework of two-color Fourier analysis to analyze this method. Our objective is to give a clearer explanation of the physical mechanism behind this method rather than to rederive the specific result obtained in [28]. We will show that the two-color two-grid iteration process asymptotically reduces to a one-color two-grid iteration process which is much easier to understand.

5.1 Framework of the two-color two-grid analysis

We summarize the two-grid iteration model, which is discussed in detail in [28], as follows. Let L_h and L_{2h} be the 5-point discretizations of the Laplacian on grids Ω_h and Ω_{2h}. Consider the full-weighting restriction operator I_h^{2h} from Ω_h to Ω_{2h} and the linear interpolation operator I_{2h}^h from Ω_{2h} to Ω_h, which are usually represented in stencil form as

$$I_h^{2h}: \left|\begin{array}{ccc} \frac{1}{16} & \frac{1}{8} & \frac{1}{16} \\ \frac{1}{8} & \frac{1}{4} & \frac{1}{8} \\ \frac{1}{16} & \frac{1}{8} & \frac{1}{16} \end{array}\right|_h^{2h}, \qquad I_{2h}^h: \left|\begin{array}{ccc} \frac{1}{4} & \frac{1}{2} & \frac{1}{4} \\ \frac{1}{2} & 1 & \frac{1}{2} \\ \frac{1}{4} & \frac{1}{2} & \frac{1}{4} \end{array}\right|_{2h}^{h}. \tag{5.1}$$

Then, a $(h,2h)$ two-grid iteration matrix with the red/black Gauss-Seidel smoothing can be written as

$$T_h^{2h} = (S_{RBGS})^{\nu_2} K_h^{2h} (S_{RBGS})^{\nu_1}, \qquad K_h^{2h} = I_h - I_{2h}^h L_{2h}^{-1} I_h^{2h} L_h, \tag{5.2}$$

where I_h is the identity matrix, ν_1 and ν_2 are the numbers of presmoothing and postsmoothing iterations. We want to determine the spectral radius $\rho(T_h^{2h})$ and, more

importantly, to explain how the two-grid iteration (5.2) works.

In the current context, (ξ,η) is nondegenerate if $1 \le \xi, \eta < \frac{M}{2}$ and degenerate if $\xi = \frac{M}{2}$ or $\eta = \frac{M}{2}$. We consider only the nondegenerate case, and the degenerate case can be treated similarly [22]. Let $\hat{e}_{\xi,\eta}$ be the Fourier coefficient of the error, and let $\hat{f}_{\xi,\eta}$ and $\hat{b}_{\xi,\eta}$ be the Fourier coefficients of the error defined at the red and black points respectively. Through the iteration (5.2), four Fourier components $\hat{e}_{\xi,\eta}$, $\hat{e}_{\xi,M-\eta}$, $\hat{e}_{M-\xi,\eta}$ and $\hat{e}_{M-\xi,M-\eta}$ with $1 \le \xi, \eta < \frac{M}{2}$, are coupled together. Hence, the spectrum of T_h^{2h} can be analyzed by focusing on a subspace spanned by these four components. Stüben and Trottenberg used the unit vector of these four Fourier components as a basis. Here, we use a different basis obtained by

$$\begin{bmatrix} \hat{f}_{\xi,\eta} \\ -\hat{f}_{\xi',\eta'} \\ \hat{b}_{\xi,\eta} \\ -\hat{b}_{\xi',\eta'} \end{bmatrix} = \frac{1}{2} \begin{bmatrix} 1 & 1 & 0 & 0 \\ 0 & 0 & -1 & -1 \\ 1 & -1 & 0 & 0 \\ 0 & 0 & -1 & 1 \end{bmatrix} \begin{bmatrix} \hat{e}_{\xi,\eta} \\ \hat{e}_{M-\xi,M-\eta} \\ \hat{e}_{\xi',\eta'} \\ \hat{e}_{M-\xi',M-\eta'} \end{bmatrix},$$

where

$$(\xi', \eta') = \begin{cases} (M-\xi, \eta) & \text{if } \xi \ge \eta \\ (\xi, M-\eta) & \text{if } \xi < \eta \end{cases}.$$

Note that the new basis is basically obtained by folding the conventional Fourier domain into two-color Fourier domain as shown in (2.4), and therefore the above transformation maps the coupled four Fourier components $\hat{e}_{\xi,\eta}$, $\hat{e}_{\xi,M-\eta}$, $\hat{e}_{M-\xi,\eta}$ and $\hat{e}_{M-\xi,M-\eta}$ into red and black waves with indices (ξ,η) and (ξ',η') (see Figure 6).

We choose the convention that each 4×4 frequency domain matrix describes a mapping from a vector space spanned by

$$(\hat{f}_{\xi,\eta}, -\hat{f}_{\xi',\eta'}, \hat{b}_{\xi,\eta}, -\hat{b}_{\xi',\eta'})^T$$

onto itself for the rest of this section. To simplify the notation, the abbreviations

$$\alpha = \frac{\cos\xi\pi h + \cos\eta\pi h}{2}, \qquad \bar{\alpha} = \frac{\cos\xi'\pi h + \cos\eta'\pi h}{2},$$

$$\beta = \cos\xi\pi h \cos\eta\pi h \ , \qquad \tilde{\beta} = \cos\xi'\pi h \cos\eta'\pi h \ ,$$

are used. We also omit the subscripts ξ, η, ξ' and η' for α, $\tilde{\alpha}$, β and $\tilde{\beta}$ and the arguments ξ, η for frequency domain matrices.

5.2 Analysis of elements for two-grid iteration

The building blocks for the two-grid iteration process (5.2) are analyzed in this section. In the two-color Fourier domain, the red/black Gauss-Seidel iteration can be represented by

$$\hat{S}_{RBGS} = \begin{bmatrix} I & 0 \\ \hat{f} & 0 \end{bmatrix} \begin{bmatrix} 0 & \hat{f} \\ 0 & I \end{bmatrix} = \begin{bmatrix} 0 & \hat{f} \\ 0 & \hat{f}^2 \end{bmatrix}, \tag{5.3}$$

where 0 is the 2×2 zero matrix, I is the 2×2 identity matrix, and

$$\hat{f} = \begin{bmatrix} \alpha & 0 \\ 0 & \tilde{\alpha} \end{bmatrix}.$$

In addition, the frequency domain matrices for operators I_h, L_h and L_{2h}^{-1} in (5.2) are

$$\hat{I}_h = \begin{bmatrix} I & 0 \\ 0 & I \end{bmatrix}, \quad \hat{L}_h = \frac{4}{h^2} \begin{bmatrix} -I & \hat{f} \\ \hat{f} & -I \end{bmatrix}, \tag{5.4a}$$

and

$$\hat{L}_{2h}^{-1} = \frac{h^2}{2\delta}, \quad \delta = 2\alpha^2 - \beta - 1 \ . \tag{5.4b}$$

In (5.3) and (5.4), there is no coupling between vectors $(\hat{r}_{\xi,\eta}, \hat{b}_{\xi,\eta})^T$ and $(\hat{r}_{\xi',\eta'}, \hat{b}_{\xi',\eta'})^T$. The coupling between them comes from the full-weighting restriction and linear interpolation operations. The decomposition, shown in Figure 7 and commonly used in the multirate signal processing context [15], is very useful for understanding the physical mechanism of interpolation and restriction operators, and for deriving their frequency domain matrices. Conceptually, we decompose the restriction procedure I_{2h}^h into two steps.

Step 1: lowpass filtering (or averaging) at every point of Ω_h, where the weighting coefficients are specified by stencil I_h^{2h} of (5.1).

Step 2: down-sampling (or injecting) values from Ω_h to Ω_{2h}.

The interpolation operator I_{2h}^{h} is also decomposed into two steps.

Step 1: up-sampling values from Ω_{2h} to Ω_h, by which we assign 0 to points which belong to $\Omega_h - \Omega_{2h}$

Step 2: lowpass filtering at every point of Ω_h, where the weighting coefficients are specified by stencil I_{2h}^{h} of (5.1).

It is relatively easy to find a frequency domain matrix representation for each of the above steps. Combining them together, we obtain

$$\hat{I}_h^{2h} = [1 \;\; 1 \;\; 0 \;\; 0] \times \frac{1}{4} \begin{bmatrix} 1+\beta & 0 & 2\alpha & 0 \\ 0 & 1+\bar{\beta} & 0 & 2\bar{\alpha} \\ 2\alpha & 0 & 1+\beta & 0 \\ 0 & 2\bar{\alpha} & 0 & 1+\bar{\beta} \end{bmatrix} = \frac{1}{4}[1+\beta \;\; 1+\bar{\beta} \;\; 2\alpha \;\; 2\bar{\alpha}] ,$$

and

$$\hat{I}_{2h}^{h} = \begin{bmatrix} 1+\beta & 0 & 2\alpha & 0 \\ 0 & 1+\bar{\beta} & 0 & 2\bar{\alpha} \\ 2\alpha & 0 & 1+\beta & 0 \\ 0 & 2\bar{\alpha} & 0 & 1+\bar{\beta} \end{bmatrix} \times \frac{1}{2} \begin{bmatrix} 1 \\ 1 \\ 0 \\ 0 \end{bmatrix} = \frac{1}{2} \begin{bmatrix} 1+\beta \\ 1+\bar{\beta} \\ 2\alpha \\ 2\bar{\alpha} \end{bmatrix} .$$

Note that in the frequency domain the down-sampling operation adds the high frequency component $-\hat{r}_{\xi',\eta'}$ to the low frequency component $\hat{r}_{\xi,\eta}$. This phenomenon is known as *aliasing* [15]. On the other hand, the up-sampling operation duplicates the low frequency component $\hat{r}_{\xi,\eta}$ in the high frequency region in the form of $-\hat{r}_{\xi',\eta'}$, which is called *imaging* [15]. The lowpass filters cascaded with the down-sampling and the up-sampling operators are basically used to reduce the aliasing and imaging effects. For example, for low frequency components with $\xi\pi h$ and $\eta\pi h$ close to 0, we have $\alpha \approx 1$, $\beta \approx 1$, $\bar{\alpha} \approx 0$, and $\bar{\beta} \approx -1$. Hence, the aliasing and imaging effects occurring between $(\hat{r}_{\xi,\eta}, \hat{b}_{\xi,\eta})^T$ and $(\hat{r}_{\xi',\eta'}, \hat{b}_{\xi',\eta'})^T$ are substantially eliminated by the associated lowpass filters.

The product $\hat{I}_{2h}^{h}\hat{I}_h^{2h}$ can be expressed as

$$\hat{I}_{2h}^{h}\hat{I}_h^{2h} = \frac{1}{8} \begin{bmatrix} \hat{F}_{11} & \hat{F}_{12} \\ \hat{F}_{21} & \hat{F}_{22} \end{bmatrix} , \qquad (5.5)$$

where

$$\hat{F}_{11} = \begin{bmatrix} (1+\beta)^2 & (1+\beta)(1+\tilde{\beta}) \\ (1+\beta)(1+\tilde{\beta}) & (1+\tilde{\beta})^2 \end{bmatrix}, \quad \hat{F}_{12} = \hat{F}_{21}^T = \begin{bmatrix} 2\alpha(1+\beta) & 2\tilde{\alpha}(1+\beta) \\ 2\alpha(1+\tilde{\beta}) & 2\tilde{\alpha}(1+\tilde{\beta}) \end{bmatrix},$$

$$\hat{F}_{22} = \begin{bmatrix} 4\alpha^2 & 4\alpha\tilde{\alpha} \\ 4\alpha\tilde{\alpha} & 4\tilde{\alpha}^2 \end{bmatrix}.$$

Therefore, from (5.2), (5.4) and (5.5), we obtain the the frequency domain matrix for the coarse-grid correction operator

$$\hat{K}_h^{2h} = \begin{bmatrix} \hat{K}_{11} & \hat{K}_{12} \\ \hat{K}_{21} & \hat{K}_{22} \end{bmatrix}, \tag{5.6}$$

where

$$\hat{K}_{11} = I - \frac{1}{4\delta}[\hat{F}_{12}\hat{J} - \hat{F}_{11}], \quad \hat{K}_{22} = I - \frac{1}{4\delta}[\hat{F}_{21}\hat{J} - \hat{F}_{22}],$$

$$\hat{K}_{12} = \frac{-1}{4\delta}[\hat{F}_{11}\hat{J} - \hat{F}_{12}], \quad \hat{K}_{21} = \frac{-1}{4\delta}[\hat{F}_{22}\hat{J} - \hat{F}_{21}].$$

The remaining task is to combine results of (5.3) and (5.6) so that the spectral radius $\rho(\hat{T}_h^{2h})$ can be determined.

5.3 Two-to-one wave reduction

The analytical determination of the eigenvalues of the two-grid iteration matrix $\hat{T}_h^{2h}$ is in general a difficult task since it is a 4×4 matrix. However, if the red/black Gauss-Seidel smoother is used, the whole process is greatly simplified. When the first partial step of the red/black Gauss-Seidel iteration, i.e. the Jacobi iteration at red points, is performed, the values of the red points are updated by the values of their neighboring black points and their original values are totally discarded. As a consequence, the computational process that follows is only determined by the initial values of the black points. This is clearly indicated by the first two zero columns in (5.3).

For the two-grid iteration process (5.2), let us temporarily consider the special case $(\nu_1,\nu_2) = (1,0)$. For such a simple case, we find that

$$\hat{T}_h^{2h} = \begin{bmatrix} 0 & \hat{K}_{11}\hat{J} + \hat{K}_{12}\hat{J}^2 \\ 0 & \hat{K}_{21}\hat{J} + \hat{K}_{22}\hat{J}^2 \end{bmatrix} \tag{5.7}$$

and the spectral radius of $\hat{T}_h^{2h}$ is

$$\rho(\hat{T}_h^{2h}) = \rho(\hat{K}_{21}\hat{J}+\hat{K}_{22}\hat{J}^2) , \tag{5.8}$$

The two-to-one color reduction is mathematically clear from equations (5.7) and (5.8), namely, that (5.8) involves the evolution of black waves only. We can interpret its corresponding physical mechanism as follows. The two-grid iteration process $\hat{T}_h^{2h}$ consists of two processes

$$\hat{T}_{12} = \hat{K}_{11}\hat{J}+\hat{K}_{12}\hat{J}^2 , \qquad \hat{T}_{22} = \hat{K}_{21}\hat{J}+\hat{K}_{22}\hat{J}^2 ,$$

which describe the evolution from $(b_{\xi,\eta},-b_{\xi',\eta'})^T$ to $(r_{\xi,\eta},-r_{\xi',\eta'})^T$ and $(b_{\xi,\eta},-b_{\xi',\eta'})^T$ respectively. Since the m-fold repetition of T_h^{2h} gives

$$[(\hat{T}_h^{2h})^m]_{12} = \hat{T}_{12}\,\hat{T}_{22}^{m-1} , \qquad [(\hat{T}_h^{2h})^m]_{22} = \hat{T}_{22}^m ,$$

the convergence of the two-grid method depends entirely on the process $\hat{T}_{22}$. Hence, the two-color two-grid iteration process (5.2) can be equivalently characterized by the black-wave two-grid iteration process.

For general (ν_1,ν_2), since

$$\rho[\hat{T}_h^{2h}(\nu_1,\nu_2)] = \rho(\hat{S}_{RBGS}^{\nu_2}\hat{K}_h^{2h}\hat{S}_{RBGS}^{\nu_1}) = \rho(\hat{K}_h^{2h}\hat{S}_{RBGS}^{\nu_1+\nu_2}) ,$$

where the last equality comes from the fact $\rho(AB) = \rho(BA)$, we can derive that

$$\rho[\hat{T}_h^{2h}(\nu_1,\nu_2)] = \rho(\hat{K}_{21}\hat{J}^{2\nu-1}+\hat{K}_{22}\hat{J}^{2\nu}) ,$$

where $\nu = \nu_1 + \nu_2$. Let us examine the matrix

$$\hat{T}_{eq} = \hat{K}_{21}\hat{J}^{2\nu-1}+\hat{K}_{22}\hat{J}^{2\nu} ,$$

which represents a one-color two-grid iteration process and, due to (5.6), can be expressed as

$$\hat{T}_{eq} = \hat{J}\hat{K}_{eq}\hat{J}^{2\nu-1} ,$$

where

$$\hat{K}_{eq} = I - \frac{1}{4\delta}\hat{J}^{-1}\hat{F}_{21}(\hat{J}^2-I) = \begin{bmatrix} 1-\frac{(1+\beta)(\alpha^2-1)}{2\delta} & -\frac{(1+\tilde{\beta})(\tilde{\alpha}^2-1)}{2\delta} \\ -\frac{(1+\beta)(\alpha^2-1)}{2\delta} & 1-\frac{(1+\tilde{\beta})(\tilde{\alpha}^2-1)}{2\delta} \end{bmatrix}$$

is the equivalent one-color coarse-grid correction operator in the frequency domain.

Since $\rho(\hat{J}\hat{K}_{eq}\hat{f}^{2\nu-1}) = \rho(\hat{K}_{eq}\hat{f}^{2\nu})$, we see that $\hat{f}^2$ can be viewed as the equivalent one-color smoother $\hat{S}_{eq}$, which corresponds to two Jacobi relaxation steps for the black component $b_{\xi,\eta}$.

5.4 The spectral radius result

The equivalent one-color two-grid iteration matrix can also be determined for the degenerate case $\xi = \frac{M}{2}$ or $\eta = \frac{M}{2}$ [22]. Then, the spectral radius of the two-grid iteration matrix can be found by solving

$$\rho(T_h^{2h}) = \max_{1\le\xi,\eta\le\frac{M}{2}} \rho(\hat{T}_{eq}) .$$

In [28], Stüben and Trottenberg reduced their analysis to the determination of the largest value among all the spectral radii of the frequency domain matrices $\hat{f}^{2\nu}\hat{K}_{eq}$. Since we have $\rho(\hat{J}\hat{K}_{eq}\hat{f}^{2\nu-1}) = \rho(\hat{f}^{2\nu}\hat{K}_{eq})$, these two different derivations lead to the same final result. A closed form of this quantity has been derived in [28] (pp. 104-108), which is summarized as follows

$$\rho[\, T_h^{2h}(\nu=\nu_1+\nu_2)\,] = \begin{cases} \frac{1}{4} & \nu = 1 \\ \frac{1}{2\nu}\left(\frac{\nu}{\nu+1}\right)^{\nu+1} & \nu \ge 2 \end{cases} \qquad (5.9)$$

In the above expression, the maximum of $\rho(T_h^{2h})$ occurs at $(\xi\pi h, \eta\pi h) = (\frac{\pi}{2},0)$ or $(0,\frac{\pi}{2})$ when $\nu = 1$ and at $(\cos^{-1}[(\frac{\nu}{\nu+1})^{1/2}] , \cos^{-1}[(\frac{\nu}{\nu+1})^{1/2}])$ when $\nu \ge 2$.

By using the two-color Fourier analysis, we can clearly see why MG with the red/black Gauss-Seidel smoother has a good convergence behavior in spite of its poor smoothing property for the high frequency components. Through the red/black Gauss-Seidel iteration, the low and high frequency components are coupled and can be equivalently formulated as the coupling between red and black waves with the same low frequency component. It turns out that only the black wave plays a role and that the low frequency component of the black wave is solved by coarse-grid correction.

Thus, we conclude that the very high frequency components, namely those with (θ,ϕ) close to (π,π), are in fact corrected at the coarse grid rather than smoothed at the fine grid. Such an explanation is difficult to obtain using the analysis given by [28].

6. Convergence rate comparison for natural and red/black orderings

6.1 SOR and SSOR methods

Fourier analysis has been used to analyze the naturally ordered SOR and SSOR iteration methods for the Poisson problem on a square with the *periodic* boundary conditions by Chan and Elman [13]. It is shown that the optimal relaxation parameters for both cases are the same,

$$\omega^*(\text{ natural ordering ; periodic b.c. }) = \frac{2}{1+2\sin(0.5\pi h)}\ , \tag{6.1}$$

and the corresponding spectral radii are

$$\rho_{SOR}(\text{ natural ordering ; periodic b.c. }) \approx 1 - 0.5\pi h\ , \tag{6.2}$$

$$\rho_{SSOR}(\text{ natural ordering ; periodic b.c. }) \approx 1 - \pi h\ . \tag{6.3}$$

For the model Dirichlet problem, Frankel derived a classical Fourier result for the SOR iteration with the natural ordering [17]. That is, the optimal relaxation parameter is

$$\omega^*(\text{ natural ordering ; Dirichlet b.c. }) = \frac{2}{1+\sin\pi h}\ , \tag{6.4}$$

and the corresponding spectral radius is

$$\rho_{SOR}(\text{ natural ordering ; Dirichlet b.c. }) \approx 1 - 2\pi h\ . \tag{6.5}$$

This result was interpreted by LeVeque and Trefethen from a tilted-grid point of view [23]. Although there is no Fourier result of the naturally ordered SSOR iteration for the Dirichlet problem, it can be shown by matrix analysis that

$$\rho_{SSOR}(\text{ natural ordering ; Dirichlet b.c. }) \le 1 - \pi h\ , \tag{6.6}$$

and that the convergence rate is not sensitive to the choice of the relaxation parameter [18][31]. Note that (6.1)-(6.3) agrees with (6.4)-(6.6) asymptotically except for the constant multiplying h in (6.2) and (6.5).

By comparing the above results with those in Section 3, we can clearly see that for the SOR iteration the red/black ordering does not effect the choice of the optimal relaxation parameters (cf. (3.5) and (6.4)) and the rate of convergence (cf. (3.6) and (6.5)). However, for the SSOR iteration, the situation changes drastically. If the

red/black ordering is used, the acceleration due to the introduction of the relaxation parameter totally disappears (cf. (3.11), (6.3) and (6.6)).

6.2 Preconditioners

Chan and Elman also applied Fourier analysis to analyze the eigenstructures of the preconditioned system with the periodic boundary conditions and the natural ordering [13]. Their results are summarized as follows,

$$\kappa(Q_S^{-1}A)(\text{ natural ordering ; periodic b.c. }) = O(\frac{1}{h}) , \tag{6.7}$$

$$\kappa(Q_I^{-1}A)(\text{ natural ordering ; periodic b.c. }) = O(\frac{1}{h^2}) , \tag{6.8}$$

$$\kappa(Q_M^{-1}A)(\text{ natural ordering ; periodic b.c. }) = \begin{cases} O(\frac{1}{h^2}) , & c = 0 \\ O(\frac{1}{h}) , & c \neq 0 \end{cases} , \tag{6.9}$$

where Q_S, Q_I and Q_M denote the SSOR, ILU and MILU preconditioning operator. Although no Fourier result for the naturally ordered Dirichlet problem is available, these results agree with the known results for the Dirichlet case (see the references of [13]) and numerical experiments indicate that the eigenstructures for the periodic and Dirichlet cases behave in a very similar way [13].

By examining (4.7), (4.9) and (4.12), we see that the preconditioned system with the red/black ordering in general does not decrease the order of the condition number of the original Laplacian. In fact, the condition number is reduced approximately by a factor 2 for SSOR, ILU and MILU preconditioners. In contrast, effective naturally ordered preconditioners such as SSOR and MILU can decrease the condition number of the Laplacian by an order of magnitude. Thus, as far as the convergence rate is concerned, a red/black preconditioned iterative method usually converges much slower than a naturally ordered preconditioned iterative method.

The condition number analysis of the red/black ordered preconditioners is consistent with the experimental results reported by Ashcraft and Grimes [5] and, to the best of our knowledge, no such analysis has been reported before.

6.3 MG method

So far, there is no exact Fourier result for the two-grid analysis of the model Dirichlet problem with the natural ordering. However, a simplified local Fourier analysis which assumes ideal interpolation and restriction operators and ignores the boundary conditions has been performed by Brandt [10]. The smoothing rate μ of one lexicographical Gauss-Seidel relaxation is found to be $\frac{1}{2}$ by such an analysis. When the total number ν of the smoothing iteration is small, we can roughly estimate the spectral radius of two-grid iteration matrix from the smoothing rate by

$$\rho_{MG} \text{ (natural ordering)} \approx \mu^{\nu} = (\frac{1}{2})^{\nu} . \qquad (6.10)$$

Therefore, from (5.9) and (6.10), we see that the red/black Gauss-Seidel smoother has a better smoothing rate than that of the lexicographical Gauss-Seidel smoother.

6.4 Summary of Comparison

The above comparison is summarized in Table 1, where N is the number of unknowns.

ordering	SOR	SSOR	PCG	MG
natural	$O(N^{1/2})$	$O(N^{1/2})$	$O(N^{1/4})$	$O(1)$
red/black	$O(N^{1/2})$	$O(N)$	$O(N^{1/2})$	$O(1)$

Table 1: Comparison of convergence rates

The spectral radii of the MG method, which are calculated by (5.9) and (6.10), are also compared below.

ordering	$\nu = 1$	$\nu = 2$	$\nu = 3$
natural	$\frac{1}{2}$	$\frac{1}{4}$	$\frac{1}{8}$
red/black	$\frac{1}{4}$	$\frac{2}{27}$	$\frac{27}{512}$

Table 2: Comparison of the spectral radii for the MG method

7. Related work

Most research work on iterative algorithms with the multicolor ordering has been focused on the SOR method. To achieve the efficiency of the SOR iteration, the determination of the optimal relaxation parameter is crucial. However, except for few simple cases such as the model Poisson problem, this is in general a difficult task. A local two-color Four analysis was proposed by Kuo, Levy and Musicus [19] to design a local relaxation scheme which uses different relaxation parameters for different finite-difference equations associated with each grid point. The four-color SOR iteration applied to the 9-point Laplacian has been independently studied by Adams, LeVeque and Young [4] and Kuo and Levy [20]. The technique used by Adams et al. is to change the variable of iteration number to a new variable known as the "data flow time" defined by Adams and Jordan [3]. By using such a technique, the multicolor ordering scheme can be related to the natural ordering scheme and then analyzed by a modified Fourier analysis. In [20], Kuo and Levy used a four-color Fourier analysis to design a two-level SOR scheme which includes an outer block SOR iteration and an inner point SOR iteration. The four-color Fourier analysis is a natural generalization of the two-color Fourier analysis presented in this paper. Besides the four-color ordering, O'Leary considered several other ordering schemes for the 9-point Laplacian and showed that the convergence rate of the SOR iteration with these orderings is no worse that that for the natural ordering [25].

8. Extensions

We can conclude our study simply as follows. Although some algorithms such as the SOR and MG methods can be reordered to get more parallelism without sacrificing their convergence rates, some algorithms such as the SSOR and preconditioned iterative methods do have a tradeoff in achieving more parallelism and faster convergence.

A natural question that arises from this research work is: what is the "intrinsic property" of these algorithms which makes them behave so differently with respect to the reordering? A better understanding of this fundamental issue should help us to know more about parallel computation and its limitation. The poor performance of the red/black SSOR, ILU, and MILU preconditioners can be partly answered by the observation that at each iteration the red/black preconditioners use only local information while the naturally ordered preconditioners do make use of some global information.

The preconditioned iterative methods such as the PCG method are among one of the most effective methods for solving elliptic PDEs in a sequential machine. However, since effective preconditioners such as the naturally ordered SSOR and MILU schemes cannot be easily parallelized, they are not as attractive for parallel computers. It is an interesting and important research topic to find preconditioners which are easily parallelizable and give satisfactory convergence rates.

References

1. L. M. Adams and J. M. Ortega, "A multi-color SOR method for parallel computation," ICASE report, 82-9, Apr. 1982.
2. L. M. Adams, "Iterative algorithms for large sparse linear systems on parallel computers," Ph.D. dissertation, University of Virginia; also published as NASA CR-166027, NASA Langley Research Center, Hampton, VA, Nov. 1982.
3. L. M. Adams and H. F. Jordan, "Is SOR color-blind," *SIAM J. Sci. Stat.*, vol. 7, no. 2, Apr. 1986.
4. L. M. Adams, R. J. LeVeque, and D. M. Young, "Analysis of the SOR iteration for the 9-point Laplacian," To appear in *SIAM J. Num. Analy.*.
5. C. C. Ashcraft and R. G. Grimes, "On vectorizing incomplete factorization and SSOR preconditioners," *SIAM J. Sci. Stat. Comput.*, vol. 9, no. 1, pp. 122-151, 1988.
6. O. Axelsson, "A generalized SSOR method," *BIT*, vol. 13, pp. 443-467, 1972.
7. O. Axelsson, "Solution of linear systems of equations: iterative methods," in *Sparse Matrix Techniques*, ed. V. A. Barker, pp. 1-51, Springer-Verlag, Berlin and New York, 1977.
8. O. Axelsson, "A survey of vectorizable preconditioning methods for large scale finite element matrix problem," Report CNA-190, Center for Numerical Analysis, Univ. of Texas, Austin, TX, 1984.
9. O. Axelsson, "A survey of preconditioned iterative methods for linear systems of algebraic equations," *BIT*, vol. 25, pp. 166-187, 1985.
10. A. Brandt , "Multi-level adaptive solutions to boundary-value problems," *Math. Comp.*, vol. 31, no. 138, pp. 333-390, Apr. 1977.
11. A. Brandt, "Multigrid solvers on parallel computers," in *Elliptic Problem Solvers*, ed. M. H. Schultz, pp. 39-83, Academic Press, Inc., New York, N.Y., 1981.
12. T. F. Chan, "Analysis of preconditioners for domain decomposition," *SIAM J. Numer. Anal.*, vol. 24, no. 2, pp. 382-390, Apr. 1987.
13. T. F. Chan and H. C. Elman, "Fourier analysis of iterative methods for elliptic problems," CAM Report 87-04, Department of Mathematics, UCLA, Feb. 1988.
14. T. F. Chan and D. C. Resasco, "A framework for the analysis and construction of domain decomposition preconditioners," in *First International Symposium on Domain Decomposition Methods for Partial Differential Equations*, pp. 217-230, SIAM, Philadelphia, PA., 1988.
15. R. E. Crochiere and L. R. Rabiner, *Multirate Digital Signal Processing*, Prentice-Hall, Inc., Englewood Cliffs, N.J., 1983.
16. T. Dupont, R. P. Kendall, and H. H. Rachford, Jr., "An approximate factorization procedure for solving self-adjoint difference equations," *SIAM J. Numer. Anal.*, vol. 5, no. 3, pp. 559-573, 1968.
17. S. P. Frankel, "Convergence rates of iterative treatments of partial differential equations," *Math. Tables Aids Comput.*, vol. 4, pp. 65-75.
18. L. A. Hageman and D. M. Young, *Applied Iterative Methods*, Academic Press, Inc. , New York, N.Y., 1981.
19. C.-C. J. Kuo, B. C. Levy, and B. R. Musicus, "A local relaxation method for solving elliptic PDEs on mesh-connected arrays," *SIAM J. Sci. Stat. Comput.*, vol. 8, no. 4, pp. 550-573, 1987.
20. C.-C. J. Kuo and B. C. Levy, "A two-level four-color SOR method," to appear in *SIAM J. Numer. Analy.*.

21. C.-C. J. Kuo, "Discretization and solution of elliptic PDEs: a transform domain approach," Ph.D. Thesis, Report LIDS-TH-1687, Laboratory for Information and Decision Systems, MIT, Cambridge, MA., Aug. 1987.

22. C.-C. J. Kuo and B. C. Levy, "Two-color Fourier analysis of the multigrid method with red/black Gauss-Seidel smoothing," CAM Report 88-02, Department of Mathematics, UCLA, Jan. 1988.

23. R. J. LeVeque and L. N. Trefethen, "Fourier analysis of the SOR iteration," Numerical Analysis Report 86-6, Department of Mathematics, MIT, Cambridge, MA., Sep. 1986.

24. J. A. Meijerink and H. A. van der Vorst, "An iterative solution method for linear systems of which the coefficient matrix is a symmetric M-Matrix," *Math. Comp.*, vol. 31, no. 137, pp. 148-162, 1977.

25. D. P. O'Leary, "Ordering schemes for parallel processing of certain mesh problems," *SIAM J. Sci. Stat. Comput.*, vol. 5, no. 3, pp. 620-632, Sep. 1984.

26. J. M. Ortega and R. G. Voigt, "Solution of partial differetial equations on vector and parallel computers," *SIAM Review*, vol. 27, no. 2, pp. 149-240, Jun. 1985.

27. Y. Saad and M. H. Schultz, "Parallel implementations of preconditioned conjugate gradient methods," Research Report YALEU/DCS/RR-425, Oct. 1985.

28. K. Stüben and U. Trottenberg, "Multigrid methods : fundamental algorithms, model problem analysis, and applications," in *Multigrid Methods*, ed. W. Hackbusch and U. Trottenberg, pp. 1-176, Springer-Verlag, New York, N.Y., 1982.

29. D. M. Young, "Iterative methods for solving partial differential equations of elliptic type," Doctoral Thesis, Harvard University, 1950.

30. D. M. Young, *Iterative Solution of Large Linear Systems*, Academic Press, Inc., New York, N.Y., 1971.

31. D. M. Young, "On the accelerated SSOR method for solving large linear systems," *Adv. in Mathematics*, vol. 23, pp. 215-271, 1977.

32. D. Young, T. Oppe, D. Kincaid, and L. Hayes, "On the use of vector computers for solving large sparse linear systems," Report CNA-199, Center for Numerical Analysis, Univ. of Texas, Austin, TX, 1984.

Figure Captions

Figure 1: (a) Conventional and (b) folded two-color Fourier domains, where $\theta = \xi\pi h$ and $\phi = \eta\pi h$.

Figure 2: (a) The eigenvalues $\lambda_{\pm}$ of the SSOR-preconditioned system as function of $\alpha_{\xi,\eta}$ and (b) the surface plot of λ_{+} as function of (θ,ϕ) with $h = 0.05$.

Figure 3: (a) The eigenvalues of the ILU-preconditioned system as function of $\alpha_{\xi,\eta}$ and (b) the surface plot of the nonconstant eigenvalue as function of (θ,ϕ) with $h = 0.05$.

Figure 4: The condition number of the MILU-preconditioned system as function of the parameter c with (a) $h = \frac{1}{5}$, (b) $h = \frac{1}{10}$, (c) $h = \frac{1}{15}$ and (d) $h = \frac{1}{20}$.

Figure 5: (a) The eigenvalues $\lambda_{\pm}$ of the MILU-preconditioned system as function of $\alpha_{\xi,\eta}$ and (b) the surface plot of λ_{+} as function of (θ,ϕ) with $h = 0.05$.

Figure 6: Four coupled Fourier components in (a) conventional and (b) two-color Fourier domains.

Figure 7: Decomposition of the (a) restriction and (b) interpolation operators.

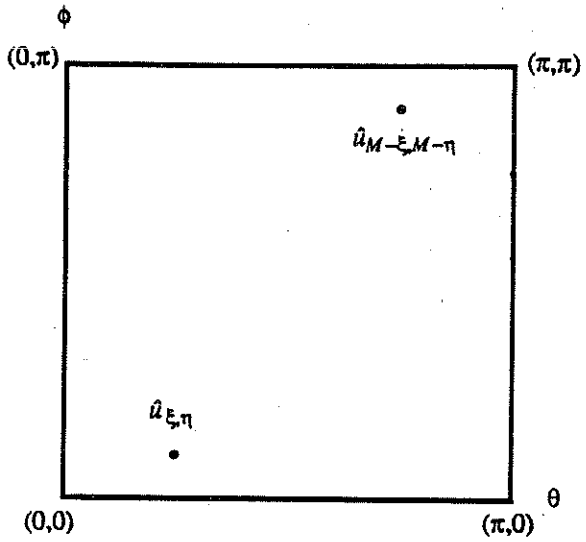

(a)

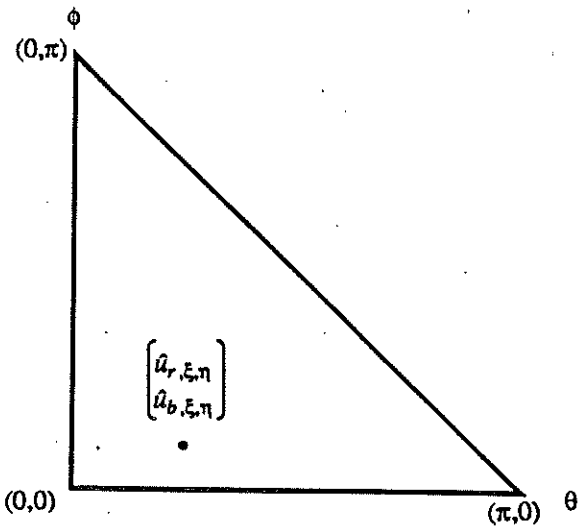

(b)

Figure 1: (a) Conventional and (b) folded two-color Fourier domains, where $\theta = \xi\pi h$ and $\phi = \eta\pi h$.

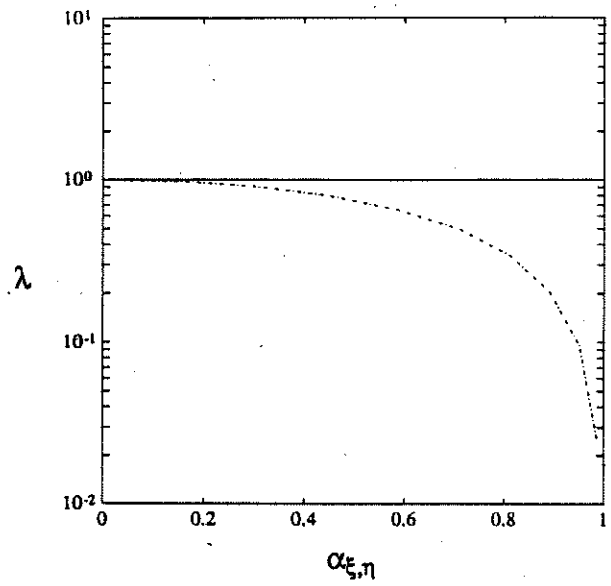

(a)

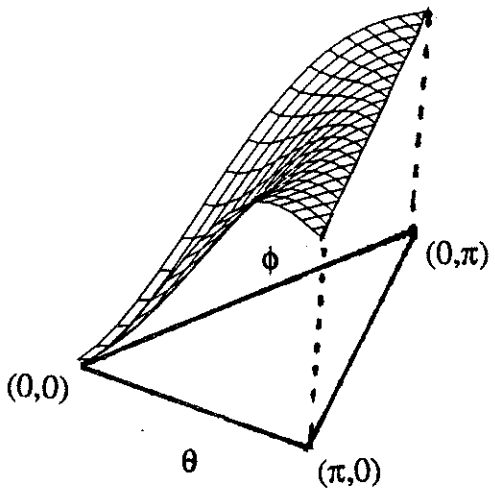

(b)

Figure 2: (a) The eigenvalues $\lambda_{\pm}$ of the SSOR-preconditioned system as function of $\alpha_{\xi,\eta}$ and (b) the surface plot of λ_{+} as function of (θ,ϕ) with $h = 0.05$.

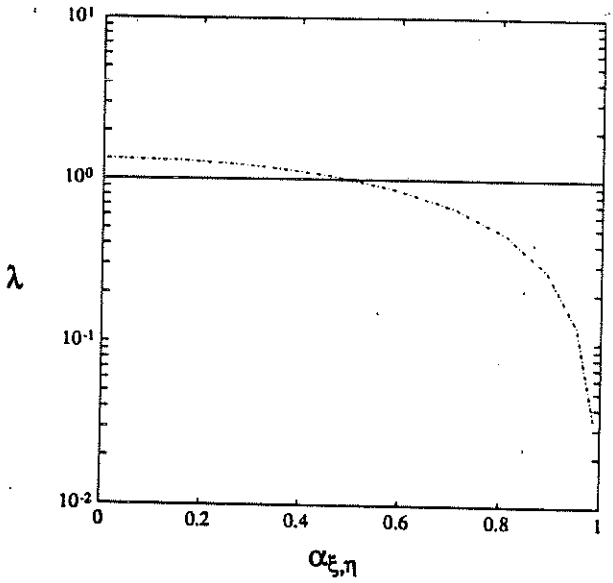

(a)

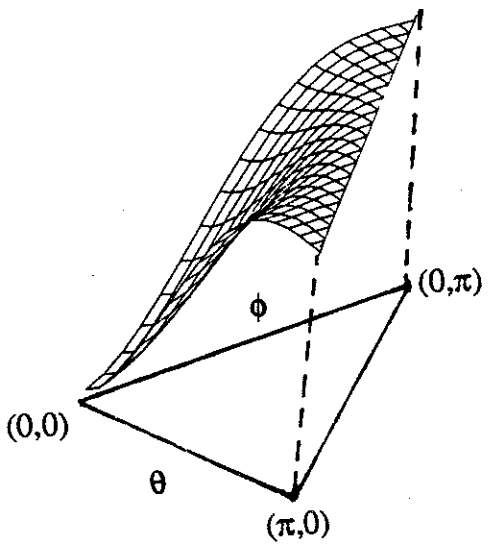

(b)

Figure 3: (a) The eigenvalues of the ILU-preconditioned system as function of $\alpha_{\xi,\eta}$ and (b) the surface plot of the nonconstant eigenvalue as function of (θ,ϕ) with $h = 0.05$.

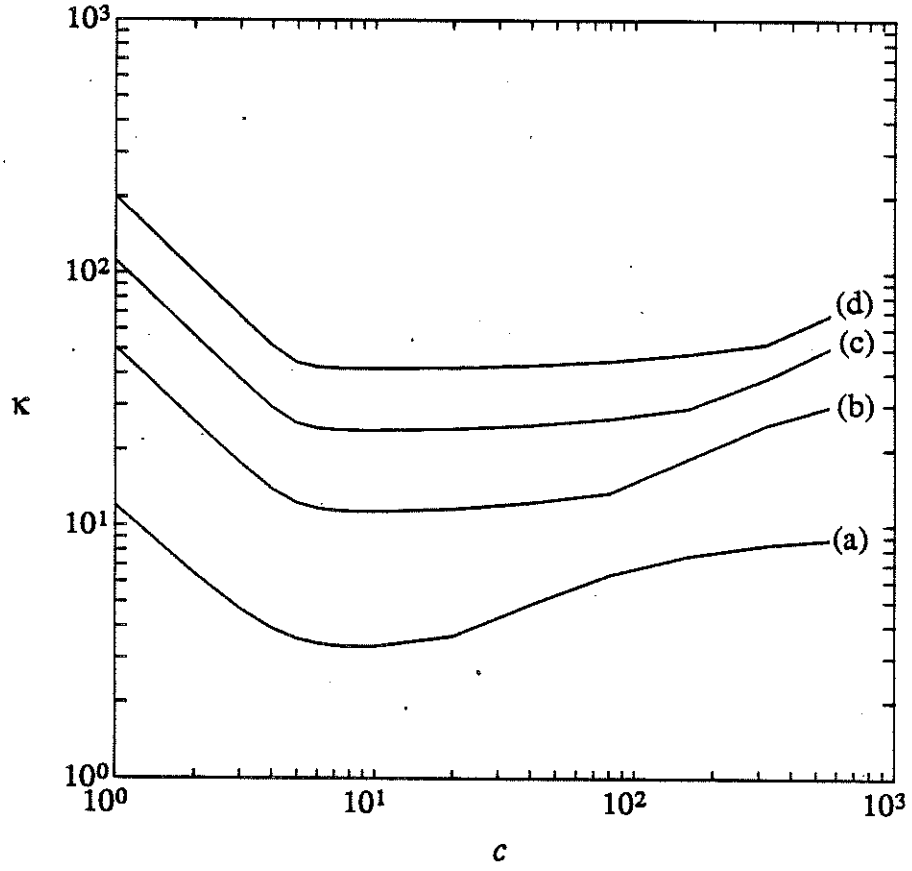

Figure 4: The condition number of the MILU-preconditioned system as function of the parameter c with (a) $h = \frac{1}{5}$, (b) $h = \frac{1}{10}$, (c) $h = \frac{1}{15}$ and (d) $h = \frac{1}{20}$.

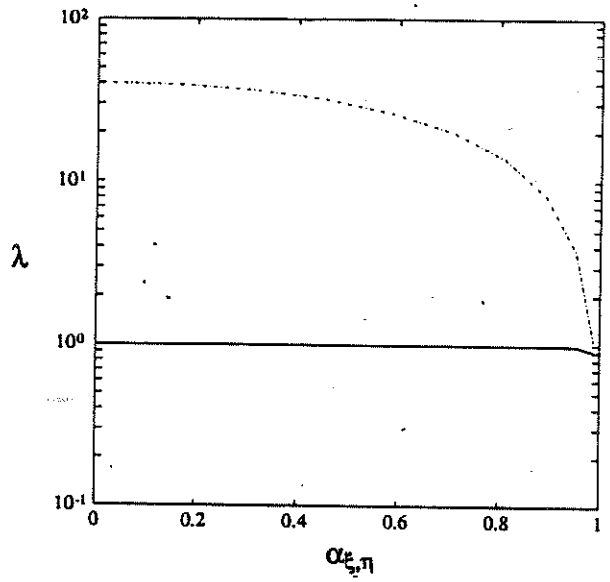

(a)

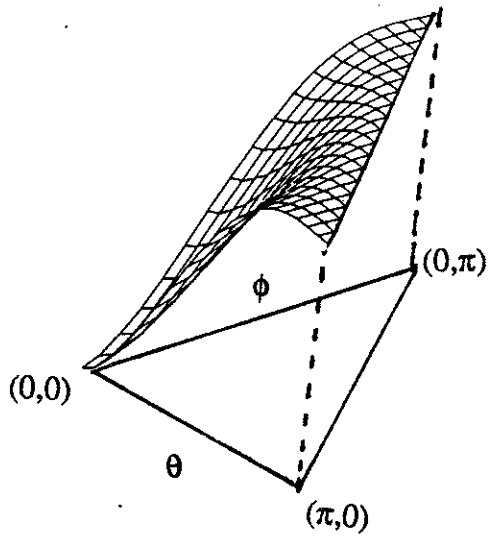

(b)

Figure 5: (a) The eigenvalues $\lambda_{\pm}$ of the MILU-preconditioned system as function of $\alpha_{\xi,\eta}$ and (b) the surface plot of λ_{+} as function of (θ,ϕ) with $h = 0.05$.

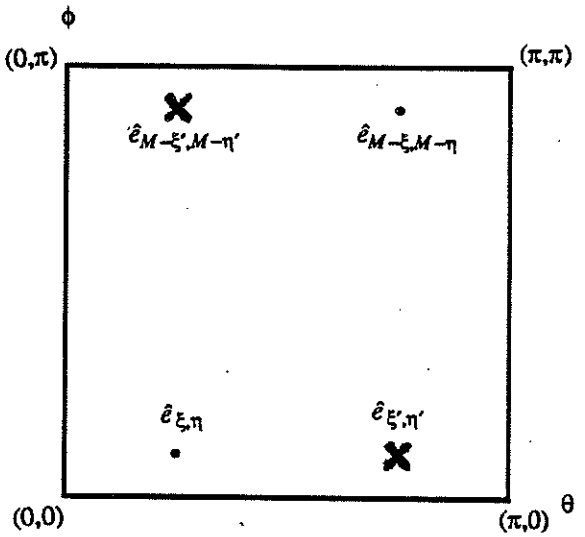

(a)

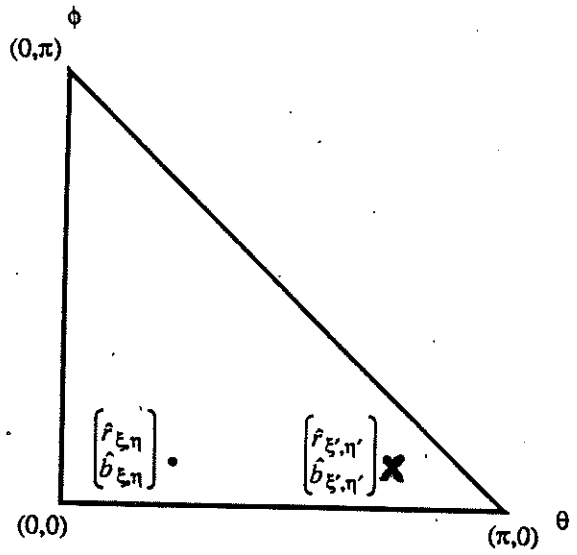

(b)

Figure 6: Four coupled Fourier components in (a) conventional and (b) two-color Fourier domains.

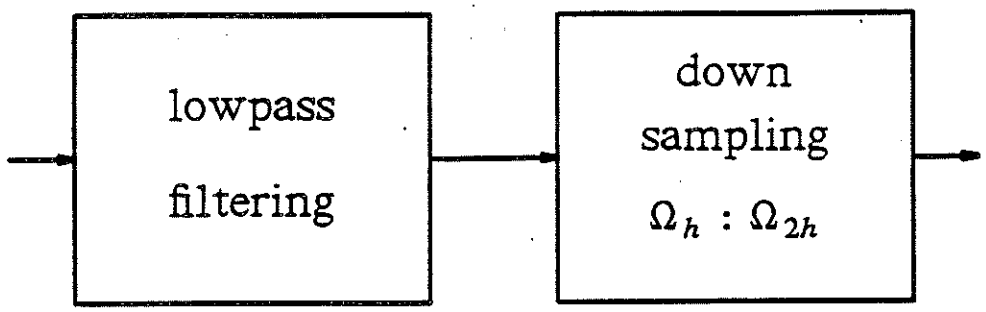

(a)

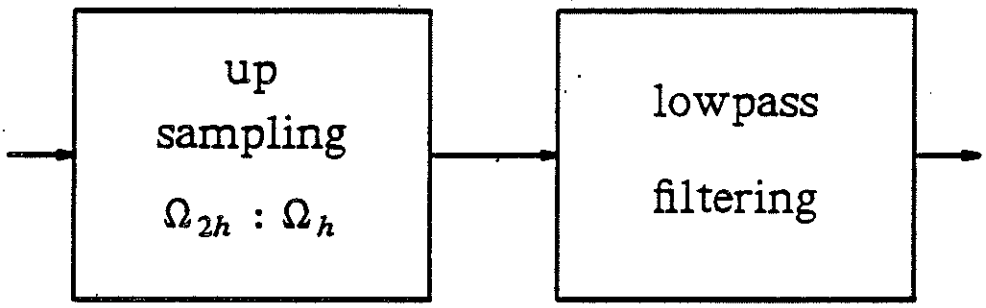

(b)

Figure 7: Decomposition of the (a) restriction and (b) interpolation operators.